NASA CONTRACTOR REPORT

NASA CR-1862

INVESTIGATION OF A HIGHLY LOADED MULTISTAGE FAN DRIVEN TURBINE

by D. C. Evans

Prepared by
GENERAL ELECTRIC COMPANY
Cincinnati, Ohio 45215
for Lewis Research Center

NATIONAL AERONAUTICS AND SPACE ADMINISTRATION • WASHINGTON, D. C. • JULY 1971

1. Report No. NASA CR-1862	2. Government Accession No.	3. Recipient's Catalog No.
4. Title and Subtitle INVESTIGATION OF A HIGHLY LOADED MULTISTAGE FAN DRIVEN TURBINE		5. Report Date July 1971 6. Performing Organization Code
7. Author(s) D. C. Evans		8. Performing Organization Report No. None
9. Performing Organization Name and Address General Electric Company Cincinnati, Ohio 45215		10. Work Unit No. 11. Contract or Grant No. NAS 3-14304
12. Sponsoring Agency Name and Address National Aeronautics and Space Administration Washington, D. C. 20546		13. Type of Report and Period Covered Contractor Report 14. Sponsoring Agency Code

15. Supplementary Notes

16. Abstract

The results of the Task I vector diagram study are presented. The effect of flowpath configuration, stage leaving swirl, work gradients, nonconstant work, stage energy split, and streamline slope and curvature were investigated. Based on these studies a particular type of vector diagram calculation was selected for the Task III turbine design.

17. Key Words (Suggested by Author(s)) Turbine High stage loading Fan engines	18. Distribution Statement Unclassified - unlimited		
19. Security Classif. (of this report) Unclassified	20. Security Classif. (of this page) Unclassified	21. No. of Pages 33	22. Price* $3.00

*For sale by the National Technical Information Service, Springfield, Virginia 22151

FOREWORD

The research described in this report was conducted by the General Electric Company under NASA contract NAS 3-14304. Mr. Thomas P. Moffitt of the Lewis Research Center Fluid System Components Division was the NASA Project Manager.

TABLE OF CONTENTS

LIST OF TABLES

LIST OF FIGURES

INTRODUCTION

The development of high-bypass-ratio turbofan engines for future aircraft propulsion schemes requires the development of fan drive turbines with increasingly higher work output. The requirements of minimized weight and size of such turbofan engines produce a need for turbines with increasingly high stage loading. In order to maintain high turbine efficiencies at high stage loading, advances are required in the technology of producing increased aerodynamic load capability in turbine blading by means of improved design techniques and high-lift devices.

The specific objectives of this program are to:

- Investigate analytically and experimentally aerodynamic means for increasing the turbine stage loading and turbine blade loading consistent with high efficiency for multistage highly loaded fan drive turbine configurations.

- Develop sufficient design information to determine the relative importance of changes in engine size, weight, and performance and give primary consideration to use of tandem rotors and stators, where applicable, to reduce weight or extend or improve the blading performance.

- Modify an existing three-stage highly loaded turbine rig and adapt the rig to an overall performance test program of sufficient extent so as to obtain blade element performance.

This is a 24-month analytical and experimental investigation program to provide a turbine high-stage-loading and high-blade-loading aerodynamic technology that will be specifically applicable to multistage fan drive turbine configurations for advanced high-bypass-ratio turbofan propulsion system application. The program will be divided into two phases encompassing nine task items of activity.

The first phase will cover Task Items I, II, and III of the program which are to investigate requirements of selected advanced high-bypass-ratio turbofan systems, to carry out parametric turbine vector diagram studies, to conduct a cascade test and evaluation program, to select one design for future study, to complete a detailed aerodynamic turbine design for an existing rig, to complete the detailed blading aerodynamic design for the rig, to perform detailed blading mechanical design for the rig, to perform the turbine rig mechanical design, and to prepare the turbine rig modification drawings required to utilize the existing three-stage highly-loaded-fan turbine rig. The second phase will cover Task Items IV through IX of this proposed program to fabricate, procure, vibration bench test, fatigue endurance test, and inspect the turbine rig modifications; to instrument and calibrate the rig vehicle; to conduct a test program and to report progress, analysis, and design, as well as test and performance results.

INTRODUCTION (Cont'd)

The purpose of this report is to present the Task I vector diagram study results.

ANALYSES AND RESULTS

Requirements

The fan turbines to be investigated in this program have the following design requirements:

Average Pitch Loading	$\frac{gJ\Delta h}{\Sigma 2U_P^2}$	1.5
Equivalent Specific Work		33.0 Btu/lb
Equivalent Rotative Speed		2000 rpm
Equivalent Weight Flow		70 lb/sec
Inlet Whirl Angle		0 degrees
Exit Whirl Angle without Guide Vanes		$\leq$ 5 degrees
Maximum Tip Diameter		45.0 inches
Number of Stages		3
$W\sqrt{T_T}/P_T$ at Inlet		108.4
$\Delta h / T_T$		.0635
$N / \sqrt{T_T}$		87.7

A vector diagram study was made to show the relationships among the turbine design options, such as flowpath, stage energy split, stage leaving swirl, and nonfree vortex work distributions for the above turbine requirements.

Three typical flowpath shapes were selected for preliminary vector diagram studies. These were:

1. Constant-inside-diameter (Figure 1)
2. Constant-outside-diameter (Figure 2)
3. Constant-pitch-diameter (Figure 3)

The flowpath diameters were determined on the basis of turbine requirements with the inlet and exit annulus areas the same for all flowpaths. The areas calculated correspond to an inlet Mach number of 0.38 and an exit Mach number of 0.40. A free-vortex vector diagram parametric study was run for the constant-inside-diameter flowpath varying the stage leaving swirl for two stage-energy extraction distributions. These calculations were made in order to determine the magnitude of the leaving swirl required to achieve a satisfactory vector diagram. The stage-energy extractions were determined by letting the third-

Requirements (Cont'd)

stage pitch aerodynamic loading $[gJ\Delta h/2U^2]$ be 0.7 with equal stage-one and -two pitch loadings in one case and equal stage-one and -two hub loadings for the second case. These results were shown for stage one, two, and three in Figures 5, 6, and 7, respectively. The vector diagram nomenclature was shown in Figure 4.

A swirl of 47 degrees on stage one yields a vector diagram which has a sonic stator hub and hence a subsonic stator for the equal stage-one and -two hub loading case. The rotor hub was also subsonic and accelerating. The swirl that yielded similar results on stage two was 44 degrees. The stage leaving swirl values that give sonic stage-one and -two stator hubs for the equal stage-one and -two pitch loading would be 44.5 degrees and 46 degrees on stage one and two, respectively. However, the stage-one rotor hub-leaving Mach number decreases from 0.9 to 0.8 and the stage-two rotor hub-leaving Mach number increases from 1.0 to 1.1. Because of the unbalanced rotor-leaving kinetic energies and the undesirable high leaving stage-two Mach numbers, the equal stage-one and -two pitch loading case was not pursued. On stage three, a value of swirl greater than zero yields a diffusing stator and rotor. The most difficult items apparent from this study was the diffusion in the third stage.

The following vector diagram calculations were made to compare the three flowpaths and investigate variations in radial work distributions and examine the effect of streamline slope and curvature. They assume stage-one leaving swirl about 46 degrees, stage-two leaving swirl about 44 degrees, and stage-three leaving swirl about 3 degrees unless otherwise stated.

Flowpath Comparison

Table I shows the free-vortex vector diagram calculation summary for the three flowpaths. For each turbine, the third-stage energy extraction was set such that the pitch aerodynamic loading $[gJ\Delta h/2U^2]$ was equal to 0.7. The remaining required energy extraction was split between stage one and two such that the hub aerodynamic loadings were equal. The only significant difference shown by this free-vortex vector diagram calculation is in the aerodynamic loading parameter. For the constant-outside-diameter flowpath, the stage-one and -two loadings were less, but the third-stage hub loading was larger than the other designs. There appears to be no real advantage favoring any one flowpath configuration over the others based on these vector diagram calculations.

With the constant-tip design flowpath, all of the area increases were taken on the hub wall which gave a wall slope of 27 degrees. The flow is expected to move radially inward in the hub region of the rotors where there is little acceleration, and in the third stage, even diffusion. Without a favorable radial gradient in static pressure to force the flow inward, the rotor hubs may separate. With the constant-hub design flowpath, all of the area increase was taken on the tip wall which gave a wall slope of 20 degrees. The flow has a natural tendency to move outward because of centrifugal effects.

ANALYSES AND RESULTS (Cont'd)

Flowpath Comparisons (Cont'd)

The third-stage diffusion problem could be helped by increasing the annulus area into the stage. This could be done easier with the constant-inside-diameter flowpath since the area change would require an increase in wall slope through the first two stages. This would make the inner wall slope with the constant-outside-diameter flowpath design even more severe than given for the conical flowpath.

In the past, many engine designs favored the constant-outside-diameter flowpath since it has higher energy extraction potential in the front stages due to the higher wheel speed of these stages. These designs generally require some sort of transition flowpath from the core turbine to the fan turbine. This transition duct adds length and weight to an engine. The trend in the design of present and advanced engines favors the constant-inside-diameter design flowpath, since this turbine can be close coupled to the core turbine using fewer stages. This saves engine length and weight.

For these reasons, the constant-inside-diameter flowpath configuration was chosen for additional vector diagram studies.

Vector Diagram Studies

Table II is a summary of the vector diagram calculation cases that were made for the constant-inside-diameter flowpath configuration. A base case vector diagram was selected with 17% of the turbine energy extraction on stage three, which corresponds to a pitch aerodynamic loading parameter of 0.7. The remaining 83% energy extraction was divided equally between stages one and two which gave equal stage-one and -two aerodynamic hub loading parameters. All of the variations of vector diagrams were compared to the base case calculation to determine the effect of a particular change.

Radial Work Gradient

Let a four-percent radial work gradient be defined as a change in Δ_{rCu} distribution with radius such that Δ_{rCu} is constant with radius, but rCu_1 is increased at the tip and decreased at the hub by four percent of the Δ_{rCu} as shown in Figure 8. This change, relative to the free-vortex calculation, increases the rotor inlet angle at the tip, decreases the rotor inlet angle at the hub, increases the stage leaving swirl at the hub, and decreases the stage leaving swirl at the tip. It does not noticeably change the vector diagram Mach numbers. Because of the increased swirl gradient at the stage exit, this would not be an advantageous vector diagram scheme for a stage with significant leaving swirls.

ANALYSES AND RESULTS (Cont'd)

Radial Work Gradient (Cont'd)

Two-percent and four-percent radial work gradient calculations were made. These were cases two and three in Table II. The detailed vector diagram data were shown in Table III for stage one, Table IV for stage two, and Table V for stage three.

Nonconstant Radial Work Gradient

Let a four-percent nonconstant radial work gradient be defined as a change in ΔrCu distribution with radius such that rCu_1 is increased at the tip and decreased at the hub by four percent of the ΔrCu with rCu_2 unchanged relative to the free-vortex calculation. The results of this change relative to the free-vortex design were shown on Figure 9. Note that this vector diagram increases the rotor inlet angle at the tip, decreases the rotor inlet angle at the hub with no change in the vector diagram exit angles. This kind of a change gives a stator and rotor with less radial twist and increases the energy extraction in the tip region where the wheel speed is the highest. Again, the vector diagram Mach numbers do not change significantly, only the vector angles.

Two-percent and four-percent nonconstant radial work gradient calculations were made. These were cases four and five in Table II. The detailed vector diagram data were shown in Table III for stage one, Table IV for stage two, and Table V for stage three.

Stage Energy Split

A change in stage energy split relative to the free-vortex base case was investigated. The energy extraction on stage three was increased from 17% of the turbine energy extraction of 20%, 23%, and 26%. Increasing the loading on stage three eases or eliminates the stage-three stator diffusion problem, but increases the rotor diffusion as shown in Figure 10. These were cases six, seven, and eight in Table II. The detailed vector diagram data were shown in Table III for stage one, Table IV for stage two, and Table V for stage three. In all of these cases, the remaining turbine energy extraction was split equally between stages one and two. The energy extraction requirements for the first two stages were less by the amount shifted to the third stage.

The effect of increasing the stage-one loading was shown in Table VI. Vector diagram calculations were made for stage-one aerodynamic loading parameters of 2.1, 2.3, and 2.5. The stage-three energy extraction was held at 17% of the turbine energy with the remaining 83% divided between stages one and two to give the desired stage-one aerodynamic loading parameter. These were cases one, eleven, and twelve in Table II. The stage-one nozzle hub goes supersonic as the energy extraction is increased beyond that required for a 2.1 aerodynamic loading parameter. In addition, the stage-one swirl increased as did the rotor exit relative Mach number. However, the stage-two stator Mach number decreased, as did the leaving swirl and rotor exit Mach number.

ANALYSES AND RESULTS (Cont'd)

Stage Energy Split (Cont'd)

It appears that the combination of increased loading (beyond 17% turbine energy extraction) on stage three, the stage-one aerodynamic loading equal to 2.1, the stage-two energy extraction reduced by the amount shifted to stage three would give a favorable vector diagram. A vector diagram was calculated with 23% turbine energy on stage three and was case 14 in Table II. The data were summarized in Table VII. It appears that putting 23% of the turbine energy on stage three went too far because of the amount of rotor hub diffusion. With a little less energy on stage three, the diffusion in the stator tip can still be avoided with less diffusion in the rotor hub. A vector diagram was calculated with 20% turbine energy on stage three and data for this case shown in Table IX (case 15, Table II). The result is a satisfactory stage one, an improved stage two relative to the base case, a diffusing stage-three rotor, but an accelerating stage-three stator.

Streamline Slope and Curvature

The effect of streamline slope and curvature on the vector diagram was calculated for both the constant-outside-diameter flowpath and the constant-inside-diameter flowpath. With the constant-inside-diameter flowpath, the rotor relative inlet and exit vector diagram angles increased at the tip and decreased at the hub as shown in Figure 11. With the constant-outside-diameter flowpath, the rotor relative inlet and exit vector diagram angles decreased at the tip and increased at the hub as shown in Figure 12. In both of these calculations, the radial distribution of the Δ_{rCu} was the same as the free-vortex base case.

Vector Diagram Calculated Efficiencies

For all of the free-vortex vector diagram calculations, an efficiency was calculated based on the following assumptions:

a) All stages use a test factor equal to 0.96. The test factor is defined as the ratio of the turbine required energy extraction to the vector diagram energy extraction.

b) Nozzle efficiencies were assumed equal to 0.97.

c) Rotor efficiencies were assumed equal to 0.95.

The calculated efficiency changes of the various vector diagram configurations would then be due to changes in stator and rotor leaving kinetic energies. These efficiencies were shown in Table VIII for all of the different stage energy distributions that were examined with the constant-inside-diameter flowpath. The more even the distribution of energy extraction among the three stages, the higher the calculated efficiency. The fact that the third-stage rotor efficiency would be decreasing as the third-stage energy extraction was increased was not reflected in these calculations; however, they do indicate how much turbine efficiency could be lost due to an inefficient third-stage rotor.

ANALYSES AND RESULTS (Cont'd)

Vector Diagram Calculated Efficiencies (Cont'd)

These efficiency calculations were not intended to be the expected efficiency of the various vector diagram calculations, only an indication of the efficiency changes.

CONCLUSIONS

Based on these vector diagram studies, it appears that the best turbine would be the constant-inside-diameter flowpath with a stage energy split (Δh stage / Δh turbine) of 41.7% on stage one, 38.3% on stage two, and 20.0% on stage three. The corresponding stage aerodynamic loading, ($gJ\Delta h/2U^2$), would be 2.1, 1.75, and 0.82 at the pitch on stages one, two, and three, respectively. Free-vortex vector diagram data for this configuration were shown in Table IX, and a scaled vector diagram shown in Figure 13. The effect of the streamline slope and curvature on the vector diagram should be included.

This is the type of vector diagram calculation that will be pursued in the Task-III (turbine design) part of the Highly Loaded Multistage Fan Drive Turbine Program.

Table I. Free-Vortex Vector Diagram Calculation Summary, Flowpath Comparison.

Parameter	Stage One			Stage Two			Stage Three		
	Const ID	Const PD	Const OD	Const ID	Const PD	Const OD	Const ID	Const PD	Const OD
$\alpha_{1H}(^\circ)$	63.5	63.7	64.0	63.6	62.6	61.8	54.9	54.0	52.8
$\alpha_{1T}(^\circ)$	57.2	58.2	59.3	55.0	54.0	52.8	42.7	40.9	37.7
$\beta_{1H}(^\circ)$	57.9	57.6	58.0	56.9	54.4	52.6	40.0	39.7	39.8
$\beta_{2H}(^\circ)$	59.6	60.0	60.3	58.6	58.8	59.1	36.2	34.2	30.5
R_{x_H}	0.06	0.09	0.07	0.25	0.35	0.39	- 0.08	-0.08	- 0.09
$\Gamma_P(^\circ)$	45.65	45.58	46.47	43.62	43.88	43.73	3.02	3.02	3.05
M_{1H}	1.05	1.06	1.12	1.02	0.93	0.87	0.74	0.72	0.69
M_{OT}	0.38	0.38	0.38	0.54	0.55	0.55	0.63	0.62	0.59
M_{1T}	0.83	0.87	0.93	0.76	0.71	0.66	0.57	0.55	0.52
M_{R1H}	0.82	0.82	0.86	0.78	0.70	0.65	0.53	0.53	0.53
M_{R2H}	0.86	0.88	0.89	1.01	1.01	0.97	0.49	0.48	0.46
M_{R1T}	0.57	0.58	0.63	0.49	0.45	0.42	0.40	0.40	0.40
M_{R2T}	0.82	0.84	0.86	0.94	0.93	0.90	0.59	0.58	0.56
$[gJ\Delta h/2U^2]_p$	2.08	2.01	1.99	1.86	1.74	1.65	0.70	0.70	0.70
$[gJ\Delta h/2U^2]_H$	2.82	2.65	2.57	2.78	2.62	2.55	1.16	1.22	1.38

Table II. Summary of Vector Diagram Calculation Cases.

(All cases are for the constant inside diameter flowpath with stage one and stage two hub loadings equal in cases 1 through 10.)

CASE	ITEM
1	Free vortex with 17% Δh on stage three
2	2% radial work gradient with $\Delta(rCu)$ = constant
3	4% radial work gradient with $\Delta(rCu)$ = constant
4	2% non-constant work with $rCu)_2$ = constant
5	4% non-constant work with $rCu)_2$ = constant
6	Free vortex with 20% Δh on stage three
7	Free vortex with 23% Δh on stage three
8	Free vortex with 26% Δh on stage three
9	Free vortex with 23% Δh on stage three and reduced swirl for stages one and two
10	23% Δh on stage three with reduced swirl and a 2% non-constant work gradient.
11	Increased loading on stage I, $\psi_P = 2.3$
12	Increased loading on stage I, $\psi_P = 2.5$
13	Streamline slope and curvature effect
14	Stage I $\psi_P = 2.1$, 23% Δh on stage three
15	Stage I $\psi_P = 2.1$, 20% Δh on stage three

The changes made in cases 2 through 15 were relative to case 1.

Table III. Stage-One Vector Diagram Data.

Parameter	CASE 1 --- FV*	2 2% NFV*	3 4% NFV	4 2% NCW*	5 4% NCW	6 20% Δh_a	7 23% Δh_a	8 26% Δh_a	9 23% Δh_a Γ=40-40-3	10 2%NCW Γ=40-40-3
$\alpha_{1H}(^\circ)$	63.5	60.9	58.5	60.9	58.5	63.4	63.2	63.0	63.5	61.1
$\alpha_{1T}(^\circ)$	57.2	59.5	62.0	59.5	62.0	57.1	56.9	56.6	57.2	59.3
$\beta_{1H}(^\circ)$	57.9	54.6	51.7	54.6	51.9	57.5	57.1	56.5	57.9	54.7
$\beta_{2H}(^\circ)$	59.6	62.7	66.1	59.6	59.6	59.5	59.3	59.1	57.8	57.8
R_{XH}	0.06	0.08	0.10	0.06	0.05	0.07	0.07	0.07	-0.09	-0.09
$\Gamma_H(^\circ)$	50.35	54.22	58.80	50.24	50.29	49.84	49.07	48.18	46.00	45.88
$\Gamma_P(^\circ)$	45.65	45.78	45.93	45.68	45.59	45.13	44.36	43.50	41.28	41.23
M_{1H}	1.05	1.04	1.03	1.05	1.05	1.02	0.98	0.95	1.05	1.04
M_{OT}	0.38	0.38	0.38	0.38	0.38	0.38	0.38	0.38	0.38	0.38
M_{1T}	0.83	0.84	0.83	0.84	0.84	0.81	0.79	0.76	0.84	0.83
M_{R1H}	0.82	0.81	0.81	0.82	0.83	0.79	0.76	0.73	0.82	0.81
M_{R2H}	0.86	0.87	0.89	0.87	0.87	0.84	0.80	0.77	0.75	0.75
M_{R1T}	0.57	0.56	0.55	0.56	0.56	0.55	0.53	0.51	0.57	0.56
M_{R2T}	0.82	0.82	0.82	0.81	0.81	0.80	0.77	0.74	0.73	0.72
$[gJ\Delta h/2U^2]_P$	2.08	2.09	2.09	2.09	2.10	2.02	1.94	1.87	1.94	1.94
$[gJ\Delta h/2U^2]_H$	2.82	2.83	2.83	2.83	2.84	2.73	2.63	2.52	2.62	2.62

* FV = Free Vortex
NFV = Nonfree Vortex
NCW = Nonconstant Work

Table IV. Stage-Two Vector Diagram Data.

Parameter	CASE 1 --- FV*	2 2% NFV*	3 4% NFV	4 2% NCW*	5 4% NCW	6 20% Δh_3	7 23% Δh_3	8 26% Δh_3	9 23% Δh_3 Γ=40-40-3	10 2%NCW Γ=40-40-3
$\alpha_{1H}(^\circ)$	63.6	60.8	58.3	60.8	58.3	63.9	64.2	64.3	64.7	62.1
$\alpha_{1T}(^\circ)$	55.0	57.3	59.7	57.3	59.7	55.4	55.7	55.8	56.3	58.5
$\beta_{1H}(^\circ)$	56.9	53.2	50.0	53.3	50.3	57.3	57.2	56.9	58.7	55.2
$\beta_{2H}(^\circ)$	58.6	61.2	64.1	58.5	58.5	59.1	59.7	60.2	58.1	58.1
R_{XH}	0.25	0.28	0.30	0.28	0.28	0.23	0.23	0.23	0.04	0.05
$\Gamma_H(^\circ)$	49.76	53.03	56.7	49.88	50.0	49.93	50.18	50.22	46.74	40.28
$\Gamma_P(^\circ)$	43.62	43.97	44.0	44.05	44.17	43.79	44.04	44.09	40.59	40.44
M_{1H}	1.02	1.01	1.00	1.02	1.03	1.01	0.97	0.93	1.06	1.04
M_{OT}	0.54	0.55	0.56	0.54	0.53	0.53	0.50	0.48	0.47	0.46
M_{1T}	0.76	0.77	0.76	0.76	0.76	0.75	0.72	0.69	0.78	0.77
M_{R1H}	0.78	0.77	0.77	0.79	0.80	0.77	0.73	0.70	0.82	0.81
M_{R2H}	1.01	1.04	1.05	1.04	1.06	0.97	0.92	0.88	0.84	0.84
M_{R1T}	0.49	0.48	0.47	0.48	0.46	0.48	0.45	0.43	0.50	0.48
M_{R2T}	0.94	0.96	0.96	0.96	0.96	0.91	0.87	0.83	0.81	0.80
$[gJ\Delta h/2U^2]_P$	1.86	1.88	1.88	1.89	1.90	1.82	1.75	1.69	1.75	1.74
$[gJ\Delta h/2U^2]_H$	2.78	2.81	2.81	2.83	2.85	2.73	2.63	2.52	2.62	2.61

* FV = Free Vortex
NFV = Nonfree Vortex
NCW = Nonconstant Work

Table V. Stage-Three Vector Diagram Data.

Parameter	CASE 1 --- FV*	2 2% NFV*	3 4% NFV	4 2% NCW*	5 4% NCW	6 20% Δh_3	7 23% Δh_3	8 26% Δh_3	9 23% Δh_3 Γ=40-40-3	10 2%NCW Γ=40-40-3
$\alpha_{1H}(^\circ)$	54.9	53.6	52.3	53.6	52.3	58.6	61.6	63.7	61.8	60.1
$\alpha_{1T}(^\circ)$	42.7	43.6	44.6	43.6	44.6	46.9	50.3	52.8	50.5	51.1
$\beta_{1H}(^\circ)$	40.0	37.8	35.8	38.5	37.3	47.5	53.0	56.9	53.2	50.52
$\beta_{2H}(^\circ)$	36.2	37.7	39.2	36.3	36.4	36.0	36.3	36.3	36.4	36.4
R_{x_H}	- 0.08	- 0.05	- 0.04	- 0.07	- 0.07	- 0.24	- 0.41	- 0.60	- 0.41	- 0.37
$\Gamma_H(^\circ)$	3.92	6.30	7.60	5.71	6.90	3.97	4.11	4.02	4.02	4.51
$\Gamma_P(^\circ)$	3.02	3.35	2.91	3.31	3.43	3.06	3.17	3.10	3.10	1.86
M_{1H}	0.74	0.73	0.72	0.75	0.77	0.86	0.97	1.10	0.97	0.94
M_{OT}	0.63	0.65	0.66	0.64	0.64	0.60	0.56	0.53	0.52	0.50
M_{1T}	0.57	0.58	0.58	0.58	0.57	0.63	0.69	0.77	0.69	0.68
M_{R1H}	0.53	0.53	0.52	0.55	0.57	0.63	0.73	0.85	0.73	0.71
M_{R2H}	0.49	0.50	0.50	0.51	0.53	0.49	0.49	0.49	0.49	0.50
M_{R1T}	0.40	0.40	0.39	0.40	0.39	0.42	0.44	0.48	0.44	0.42
M_{R2T}	0.59	0.60	0.59	0.59	0.58	0.59	0.59	0.59	0.59	0.58
$[gJ\Delta h/2U^2]_P$	0.70	0.71	0.70	0.71	0.71	0.82	0.95	1.07	0.95	0.92
$[gJ\Delta h/2U^2]_H$	1.16	1.18	1.16	1.18	1.18	1.36	1.57	1.77	1.57	1.53

* FV = Free Vortex
NFV = Nonfree Vortex
NCW = Nonconstant Work

Table VI. Increased Loading on Stage One.

Parameter	Case								
	Stage One			Stage Two			Stage Three		
	1 $\psi_{P1}=2.1$	11 $\psi_{P1}=2.3$	12 $\psi_{P1}=2.5$	1 $\psi_{P1}=2.1$	11 $\psi_{P1}=2.3$	12 $\psi_{P1}=2.5$	1 $\psi_{P1}=2.1$	11 $\psi_{P1}=2.3$	12 $\psi_{P1}=2.5$
$\alpha_{1H}(°)$	63.5	63.5	63.1	63.6	61.6	59.2	54.9	54.4	54.1
$\alpha_{1T}(°)$	57.2	57.2	56.8	55.0	52.7	50.0	42.7	42.2	41.9
$\beta_{1H}(°)$	57.9	58.8	59.0	56.9	54.1	50.2	40.0	39.5	39.2
$\beta_{2H}(°)$	59.6	59.6	58.9	58.6	56.7	54.8	36.2	35.7	35.6
R_{X_H}	0.06	0.07	0.07	0.25	0.24	0.24	- 0.08	- 0.08	- 0.08
$\Gamma_H(°)$	50.4	51.6	51.9	49.8	46.6	43.0	3.9	3.9	3.9
$\Gamma_P(°)$	45.7	47.0	47.3	43.6	40.4	36.9	3.0	3.0	3.0
M_{1H}	1.05	1.15	1.26	1.02	0.98	0.91	0.74	0.75	0.75
M_{OT}	0.38	0.38	0.38	0.54	0.62	0.70	0.63	0.60	0.56
M_{1T}	0.83	0.91	0.99	0.76	0.74	0.70	0.57	0.58	0.58
M_{R1H}	0.82	0.91	1.01	0.78	0.74	0.68	0.53	0.54	0.54
M_{R2H}	0.86	0.97	1.08	1.01	0.94	0.87	0.49	0.50	0.50
M_{R1T}	0.57	0.63	0.71	0.49	0.48	0.46	0.40	0.41	0.41
M_{R2T}	0.82	0.90	0.99	0.94	0.89	0.84	0.59	0.59	0.60
$[gJ\Delta h/2U^2]_P$	2.08	2.30	2.50	1.86	1.71	1.52	0.70	0.70	0.70
$[gJ\Delta h/2U^2]_H$	2.82	3.11	3.38	2.78	2.55	2.28	1.16	1.16	1.16

Table VII. Vector Diagram Data Case 14.

Parameter	Case					
	Stage One		Stage Two		Stage Three	
	Case 1 $\psi_{P1}=2.1$	14 $\psi_{P1}=2.1$	1 $\psi_{P2}=1.85$	14 $\psi_{P2}=1.63$	1 $\psi_{P3}=0.7$	14 $\psi_{P3}=0.95$
$\alpha_{1H}(°)$	63.5	63.5	63.6	62.7	54.9	61.1
$\alpha_{1T}(°)$	57.2	57.2	55.0	54.0	42.7	50.2
$\beta_{1H}(°)$	57.9	57.9	56.9	54.8	40.0	52.9
$\beta_{2H}(°)$	59.6	59.6	58.6	58.6	36.2	36.2
R_{X_H}	0.06	0.06	0.25	0.24	- 0.08	- 0.41
$\Gamma_H(°)$	50.4	50.4	49.8	47.9	3.9	4.1
$\Gamma_P(°)$	45.7	45.7	43.6	41.7	3.0	3.2
M_{1H}	1.05	1.05	1.02	0.92	0.74	0.97
M_{OT}	0.38	0.38	0.54	0.54	0.63	0.54
M_{1T}	0.83	0.83	0.76	0.69	0.57	0.69
M_{R1H}	0.82	0.82	0.78	0.69	0.53	0.73
M_{R2H}	0.86	0.86	1.01	0.87	0.49	0.49
M_{R1T}	0.57	0.57	0.49	0.43	0.40	0.44
M_{R2T}	0.82	0.82	0.94	0.83	0.59	0.59
$[gJ\Delta h/2U^2]_P$	2.08	2.08	1.86	1.63	0.70	0.95
$[gJ\Delta h/2U^2]_H$	2.82	2.82	2.78	2.44	1.16	1.57

Table VIII. Computer Calculated Efficiencies.

ASSUMPTIONS:

- Free-Vortex Computer Calculation
- All Stages Use A Test Factor Equal to 0.96
- Nozzle Efficiencies Assumed Equal to 0.97
- Rotor Efficiencies Assumed Equal to 0.95
- Constant-Inside-Diameter Flowpath

Case	Energy Split, Percent			Stage Pitch Loading, $gJ\Delta h/2U^2$			η_T/T Percent
	Stage			Stage			
	1	2	3	1	2	3	
1	41.7	41.2	17.1	2.08	1.85	0.70	88.7
6	40.0	40.0	20.0	2.02	1.82	0.82	89.0
7	38.5	38.5	23.0	1.94	1.75	0.95	89.3
8	37.0	37.0	26.0	1.87	1.69	1.07	89.5
11	45.6	37.4	17.0	2.30	1.71	0.70	88.5
12	49.6	33.4	17.0	2.50	1.52	0.70	88.1
14	41.3	35.7	23.0	2.08	1.63	0.95	89.2
15	41.7	38.3	20.0	2.10	1.75	0.82	89.0

Table IX. Stage One ψ_P = 2.1, 20% Δh on Stage Three.

Parameter	Stage One	Stage Two	Stage Three
$\alpha_{1H}(^\circ)$	63.0	63.6	59.0
$\alpha_{1T}(^\circ)$	56.7	54.9	47.3
$\beta_{1H}(^\circ)$	57.1	56.8	48.2
$\beta_{2H}(^\circ)$	59.0	57.3	36.2
R_{X_H}	0.07	0.11	-0.24
$\Gamma_H(^\circ)$	50.0	46.6	3.9
$\Gamma_P(^\circ)$	45.3	40.4	3.0
M_{1H}	1.05	1.03	0.85
M_{OT}	0.38	0.55	0.55
M_{1T}	0.84	0.77	0.62
M_{R1H}	0.82	0.80	0.62
M_{R2H}	0.87	0.88	0.49
M_{R1T}	0.58	0.50	0.40
M_{R2T}	0.82	0.84	0.58
$[gJ\Delta h/2U^2]_P$	2.10	1.75	0.82
$[gJ\Delta h/2U^2]_H$	2.83	2.61	1.36

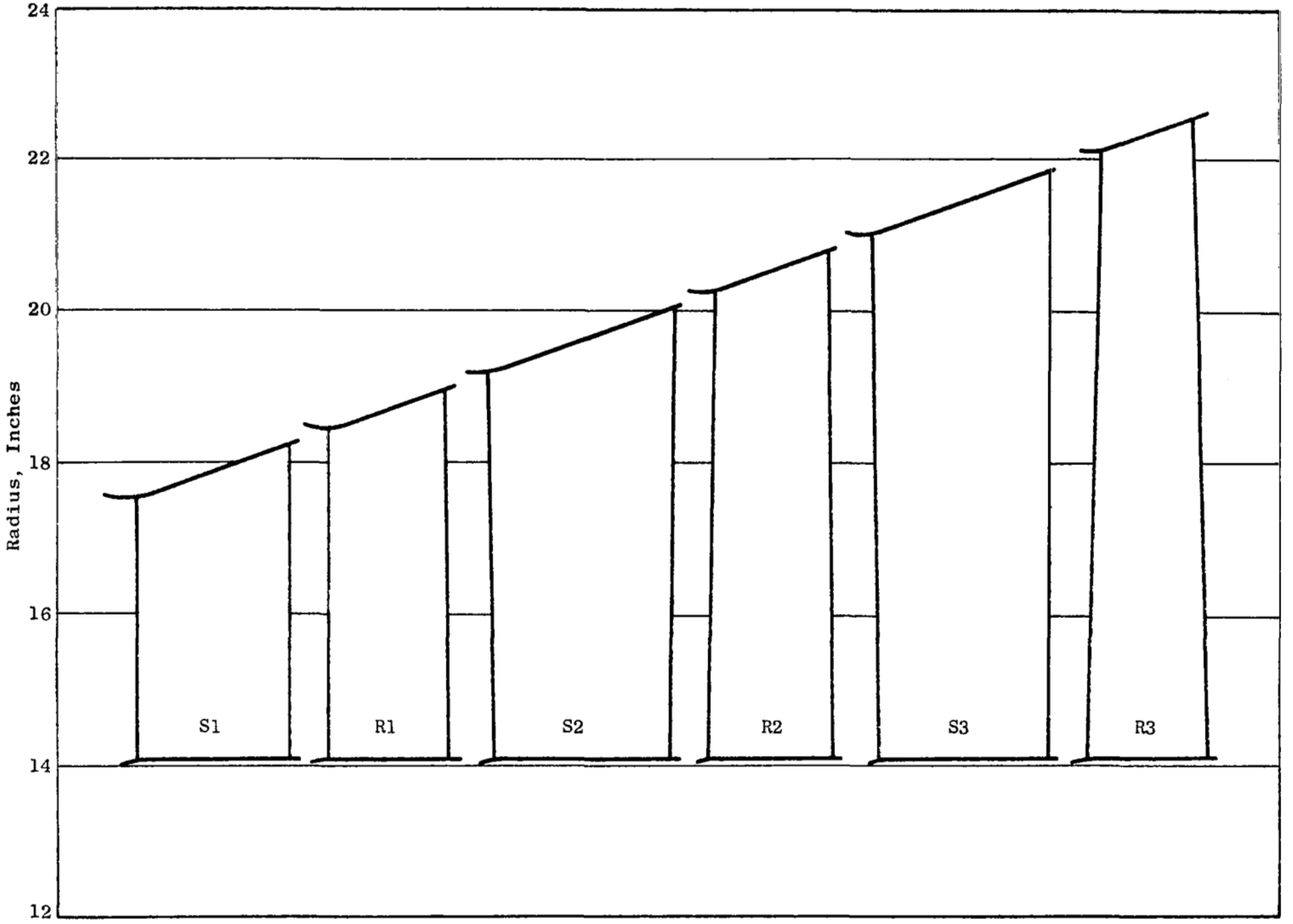

Figure 1. Flowpath, Constant-Inside-Diameter.

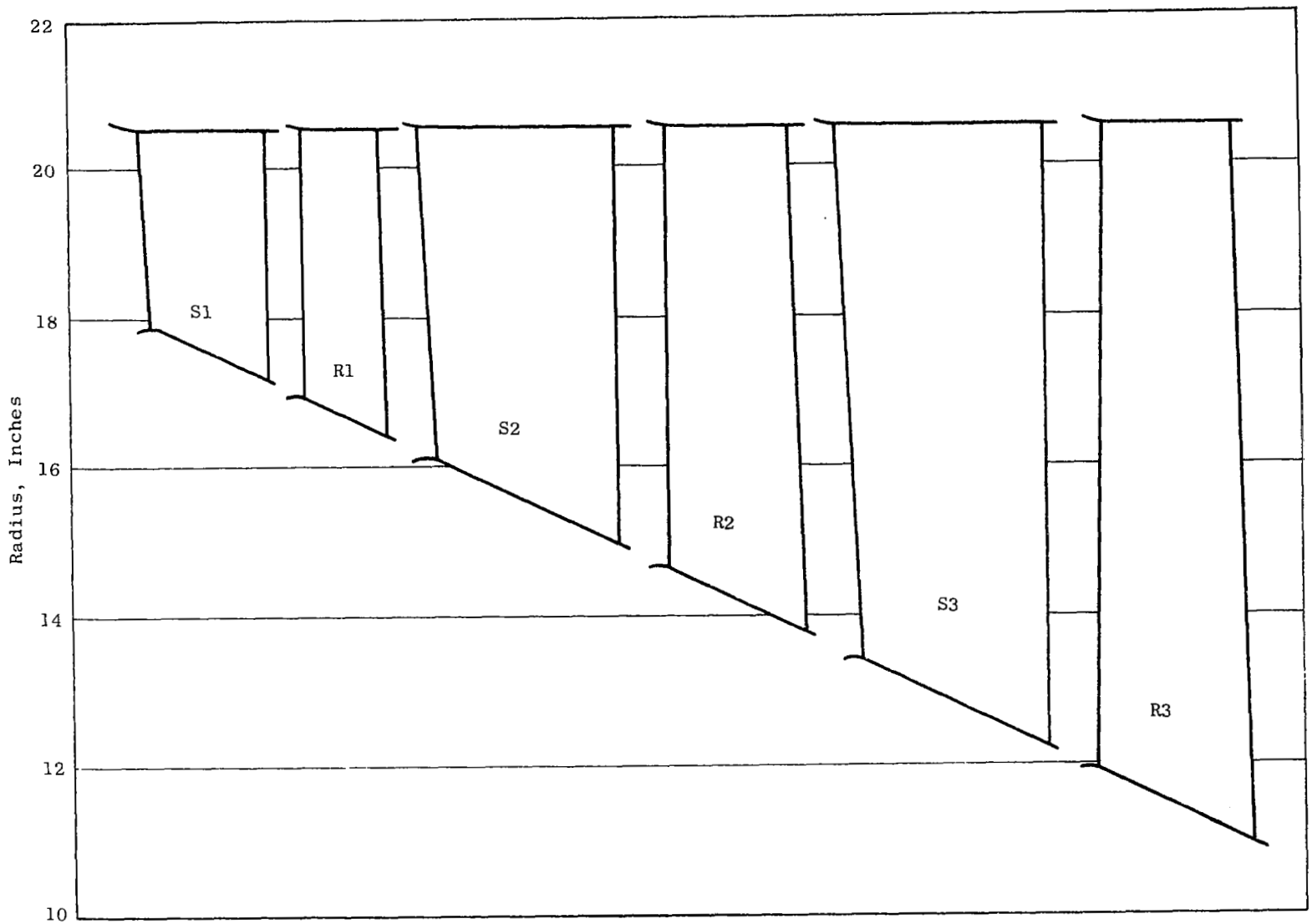

Figure 2. Flowpath, Constant-Outside-Diameter.

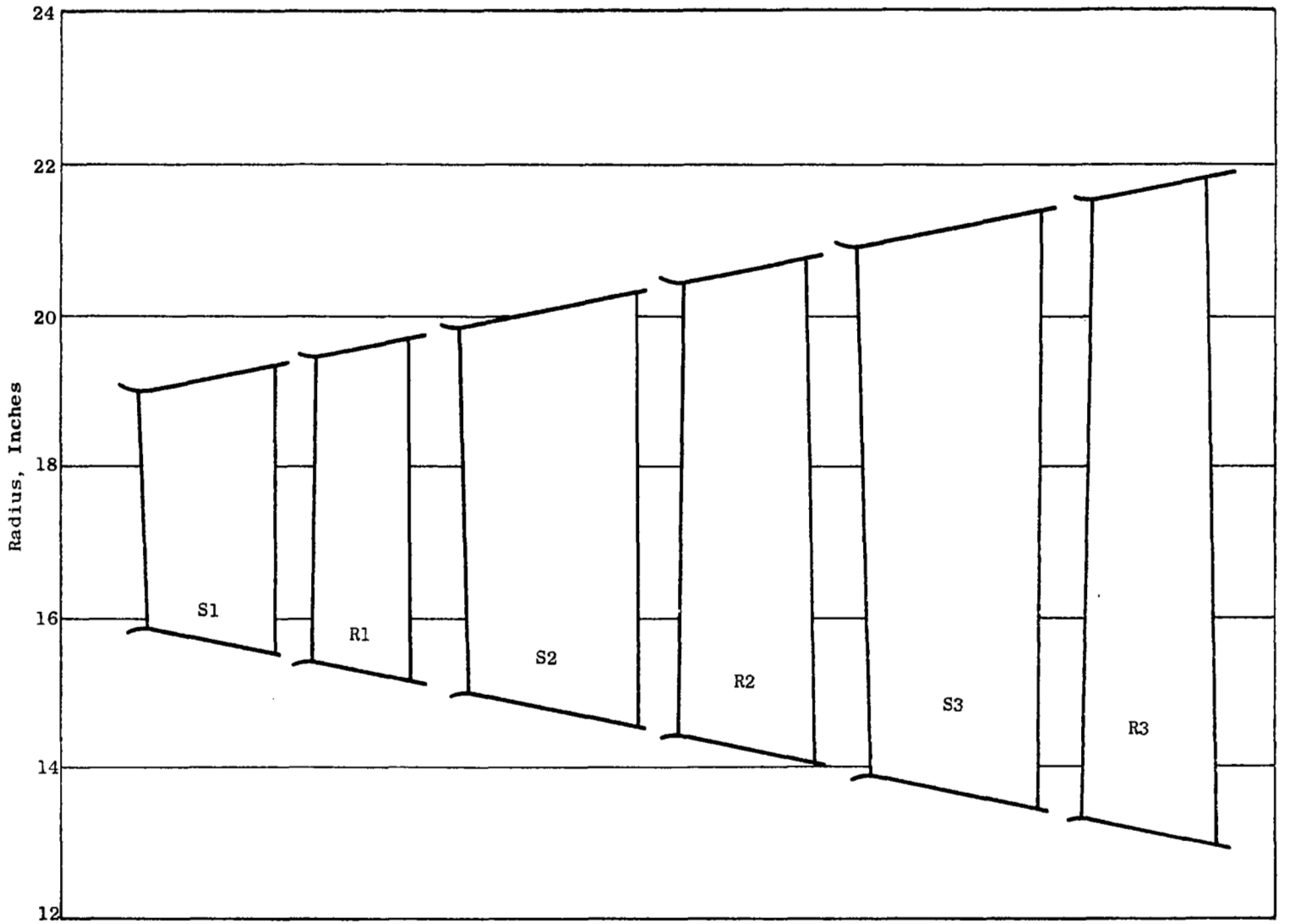

Figure 3. Flowpath, Constant-Pitchline-Diameter.

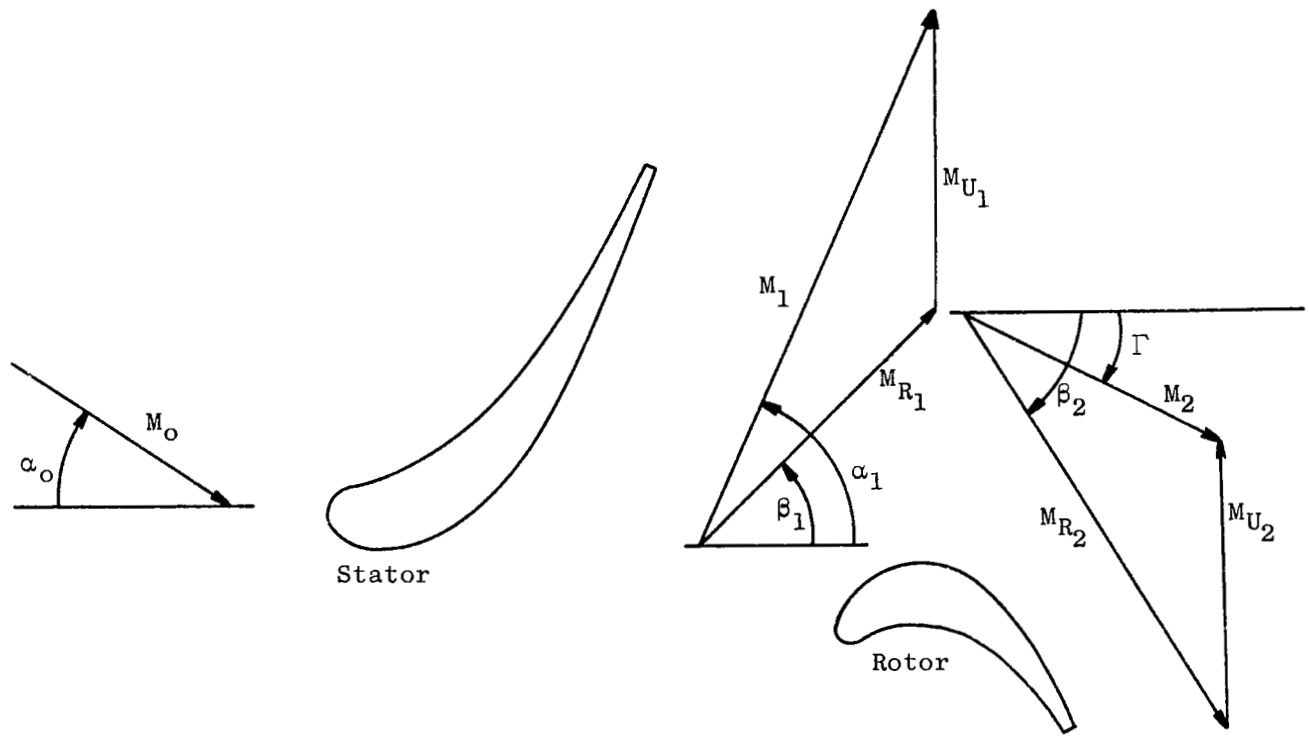

Figure 4. Vector Diagram Nomenclature.

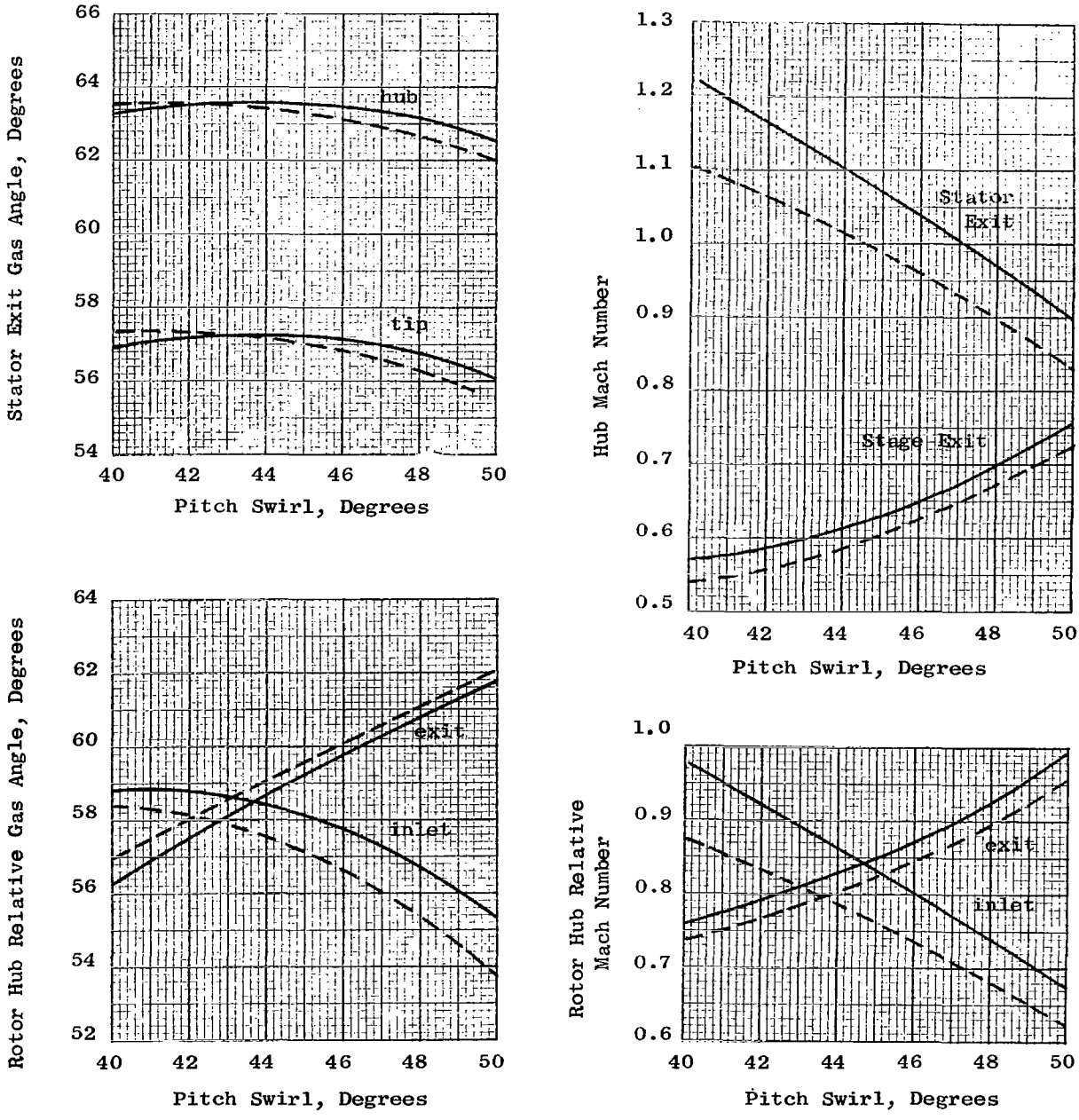

Solid lines have pitch loading ($gJ\Delta h/2U^2$) of 2.1, 1.89, and 0.7 on stages one, two, and three, respectively, which correspond to equal hub loading on stages one and two. Dashed lines have pitch loading of 1.98, 1.98, and 0.7, which correspond to hub loadings of 2.68, 2.97, and 1.16, respectively.

Figure 5. Stage-One Vector Diagram Parameters as a Function of Stage Leaving Swirl for the Constant-Inside-Diameter Flowpath.

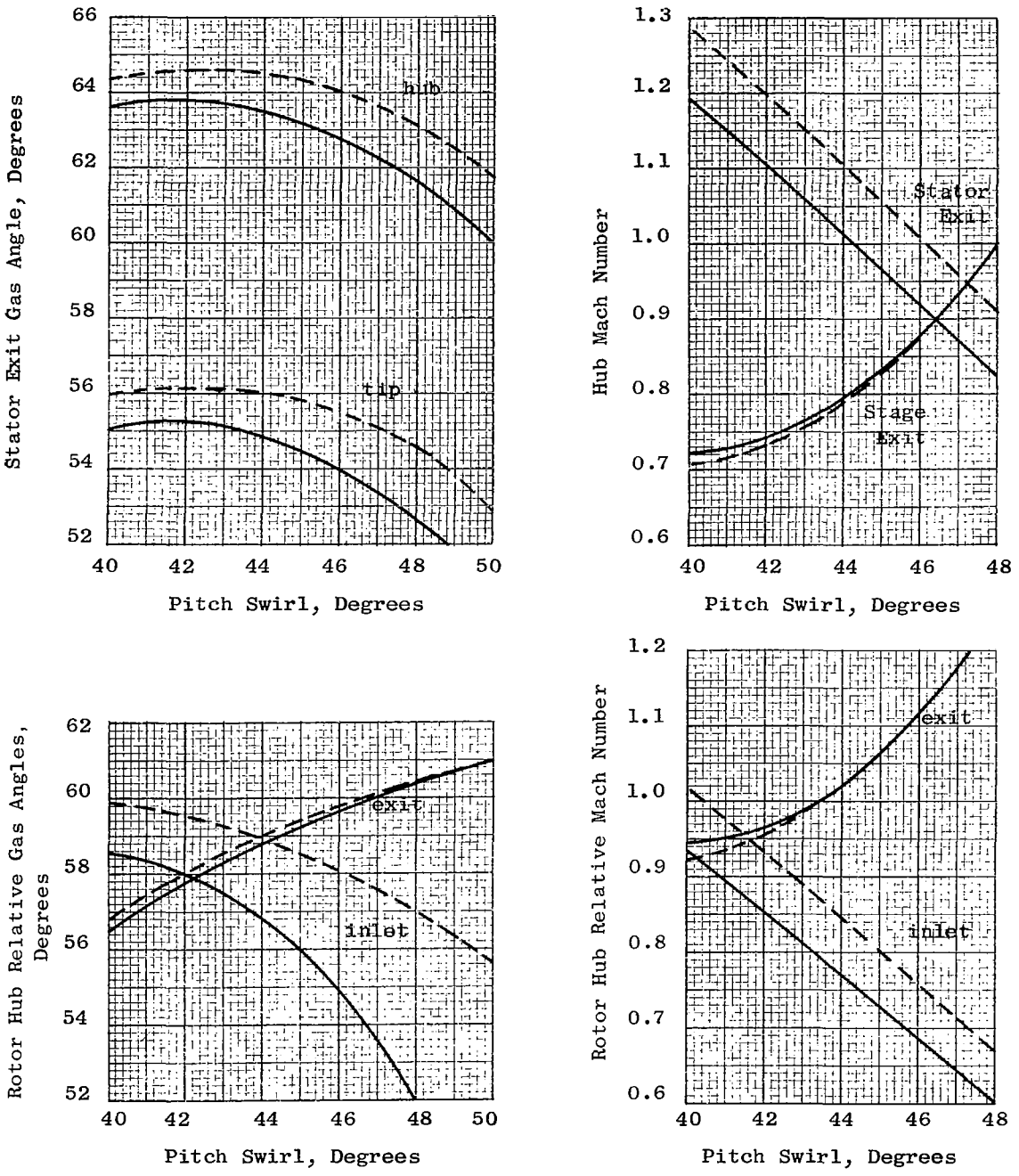

Solid lines have pitch loading ($gJ\Delta h/2U^2$) of 2.1, 1.89, and 0.7 on stages one, two, and three, respectively, which correspond to equal hub loading on stages one and two. Dashed lines have pitch loading of 1.98, 1.98, and 0.7, which correspond to hub loadings of 2.68, 2.97, and 1.16, respectively.

Figure 6. Stage-Two Vector Diagram Parameters as a Function of Stage Leaving Swirl for the Constant-Inside-Diameter Flowpath.

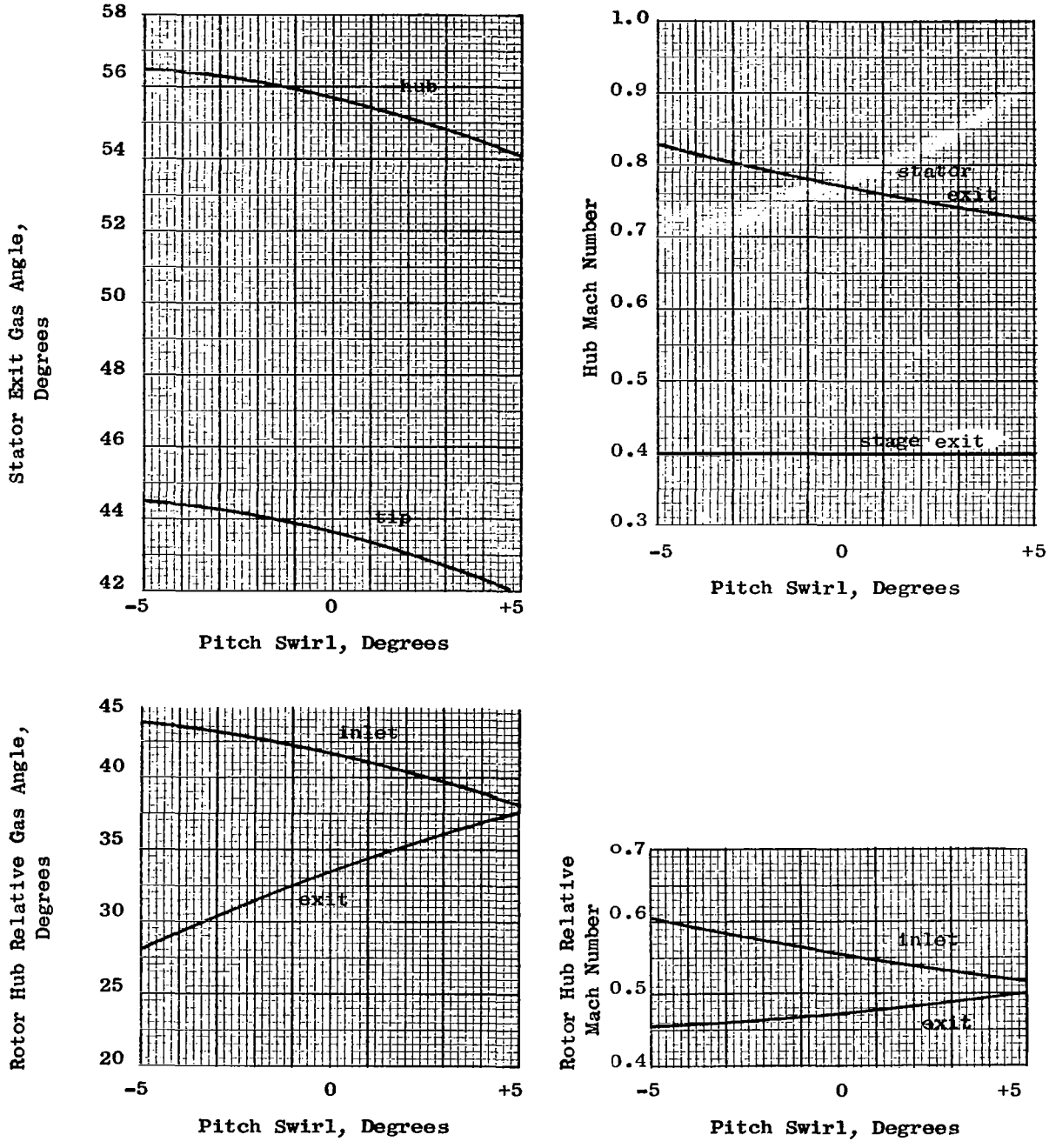

Solid lines have pitch loading ($gJ\Delta h/2U^2$) of 2.1, 1.89, and 0.7 on stages one, two, and three, respectively, which correspond to equal hub loading on stages one and two.

Figure 7. Stage-Three Vector Diagram Parameters as a Function of Stage Leaving Swirl for the Constant-Inside-Diameter Flowpath.

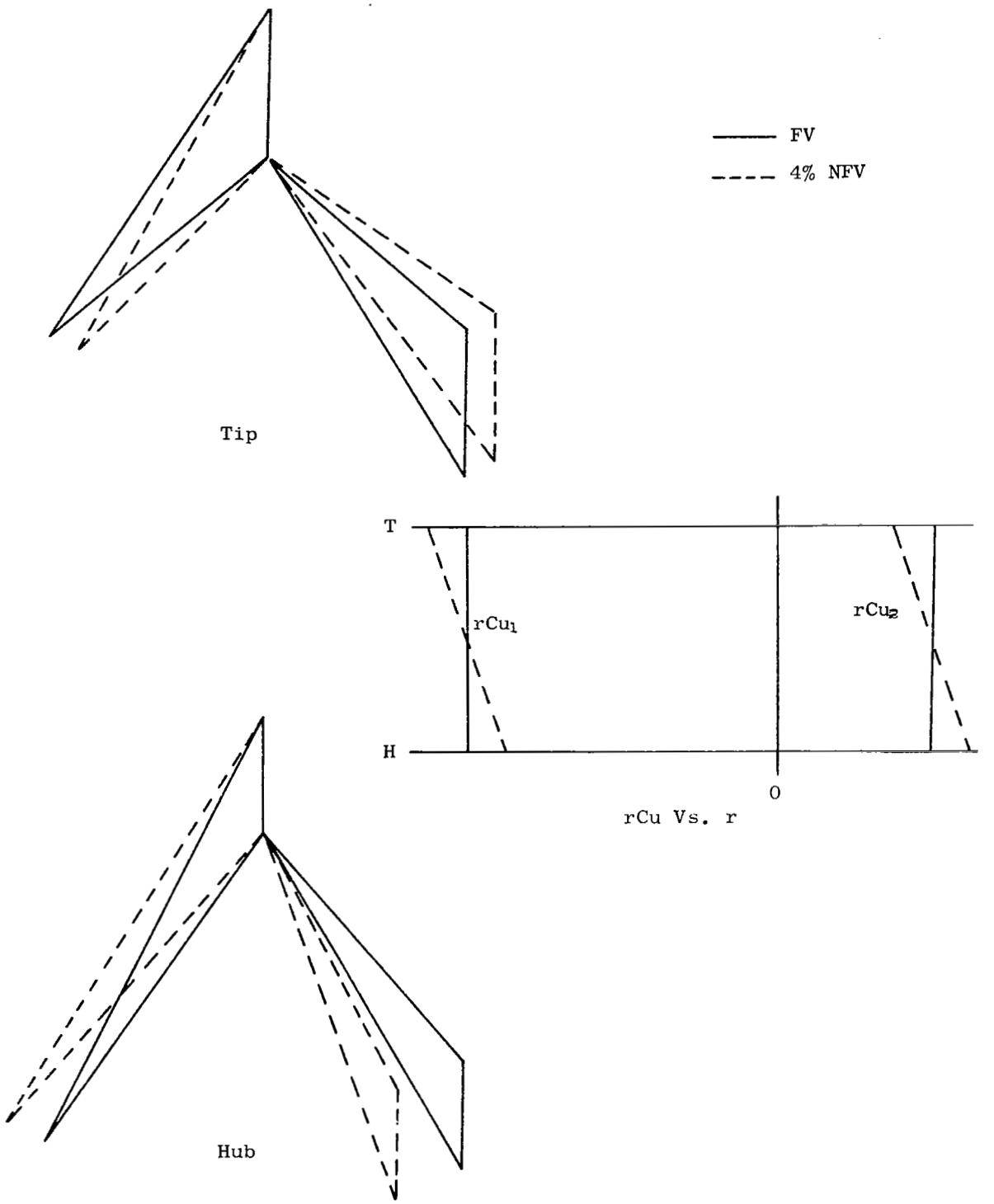

Figure 8. Constant Δ(rCu) Nonfree Vortex with Work Gradient Compared to Free Vortex for Typical Stage One, Constant-Inside-Diameter Flowpath.

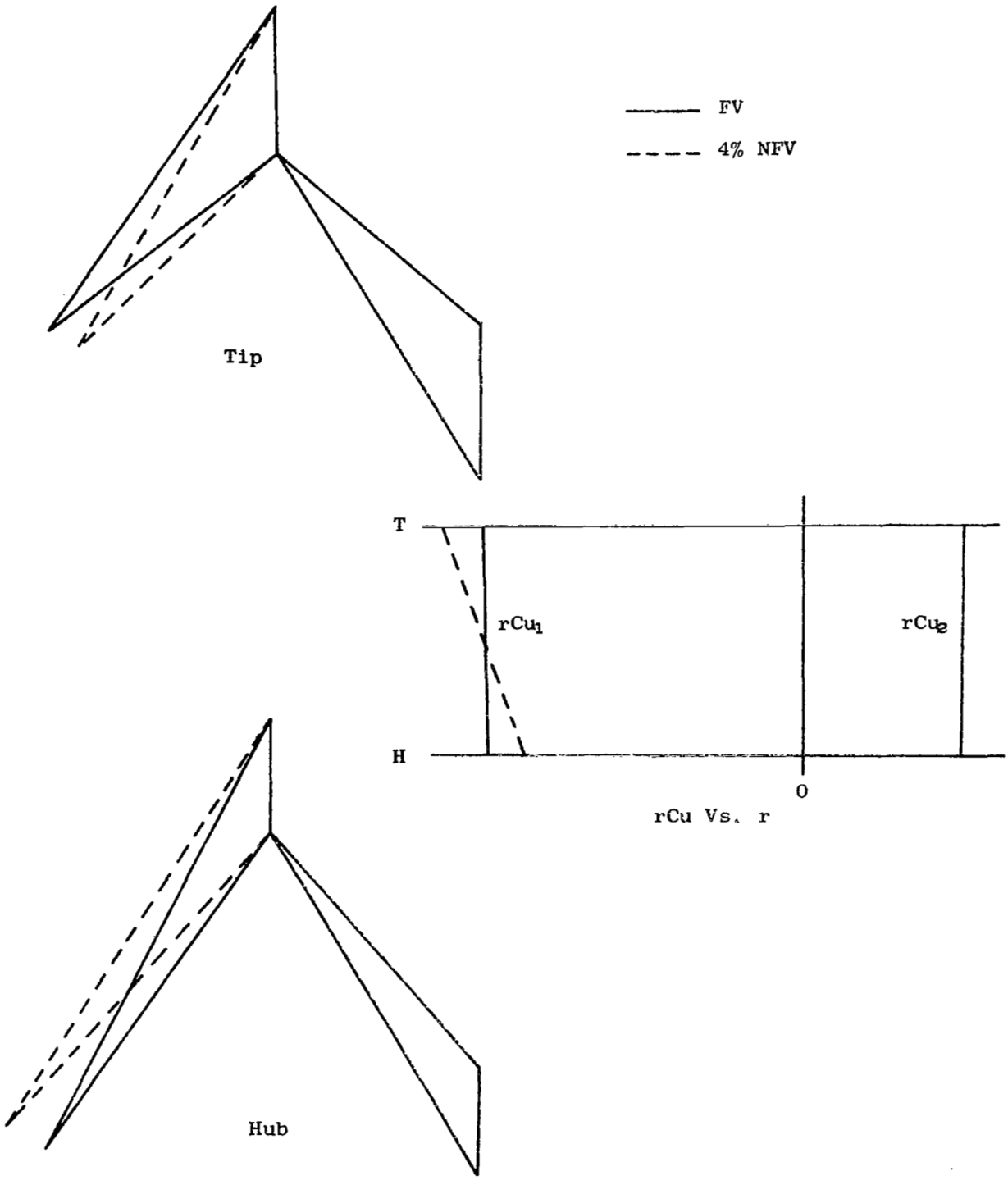

Figure 9. Nonconstant Work Vector Diagram Compared to Free Vortex for Typical Stage One, Constant-Inside-Diameter Flowpath.

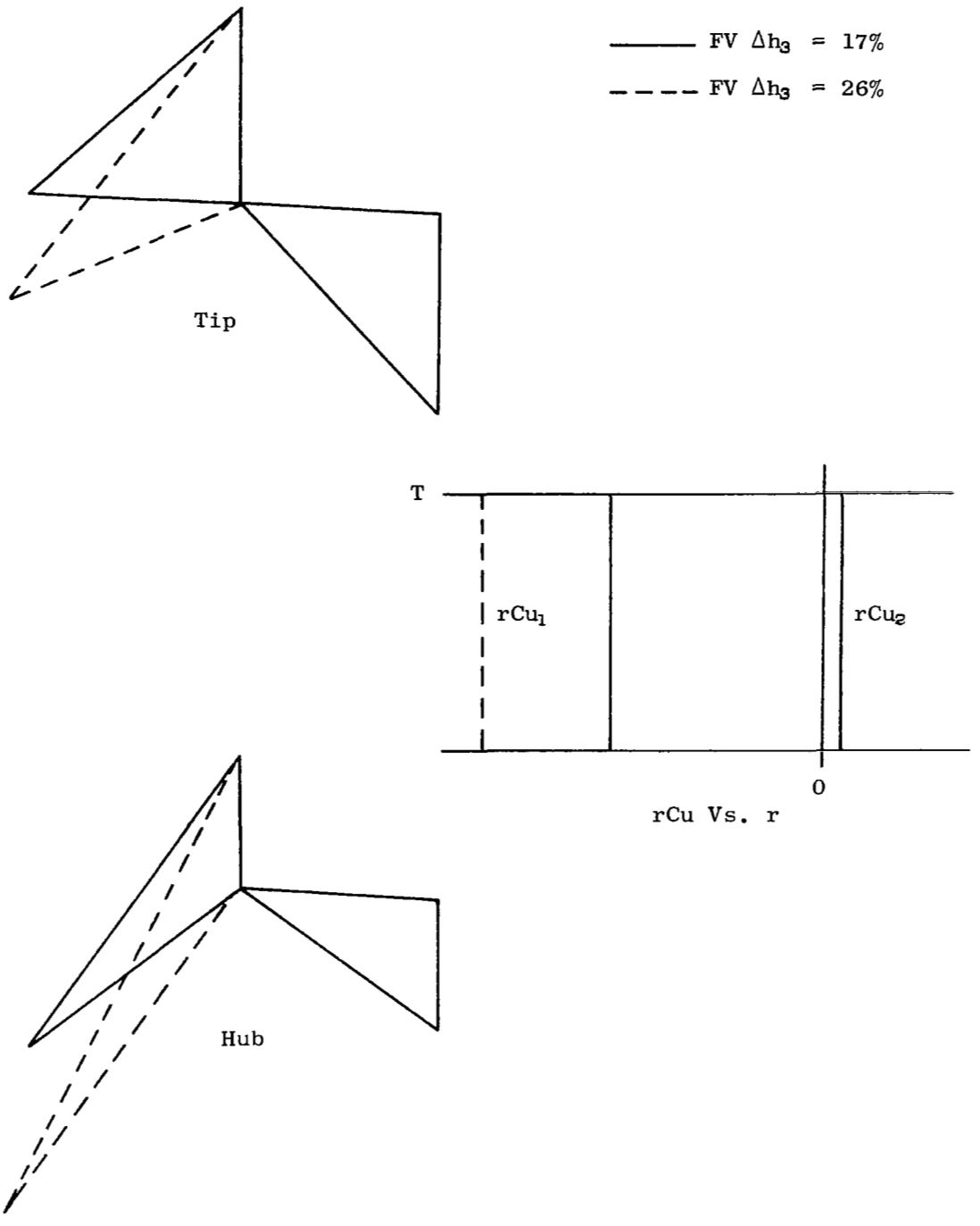

Figure 10. Highly Loaded Stage Three Compared to Conventionally Loaded Free-Vortex Stage Three, Constant-Inside-Diameter Flowpath.

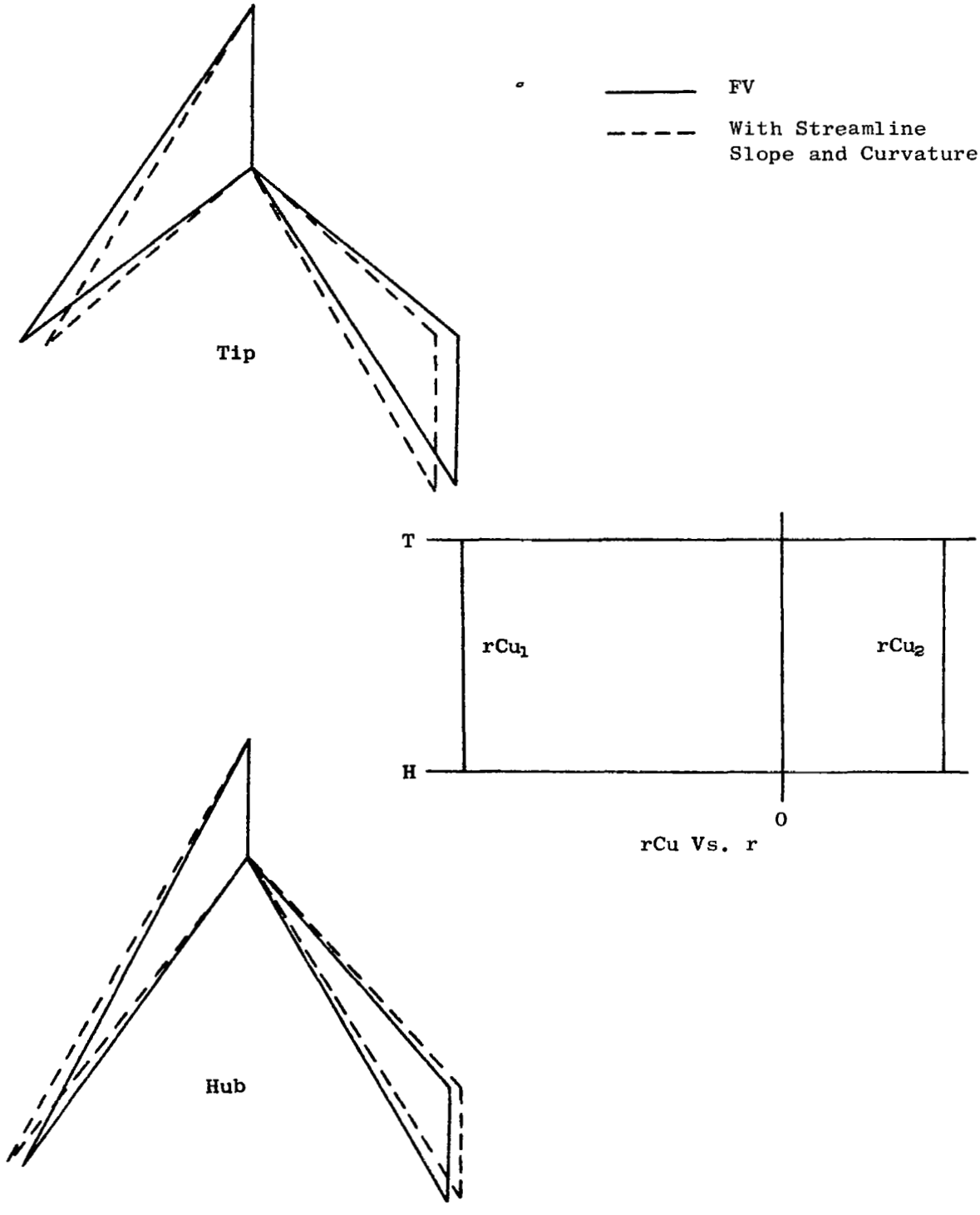

Figure 11. Constant-Inside-Diameter Flowpath Streamline Slope and Curvature Effect Compared to Free Vortex for Typical Stage One.

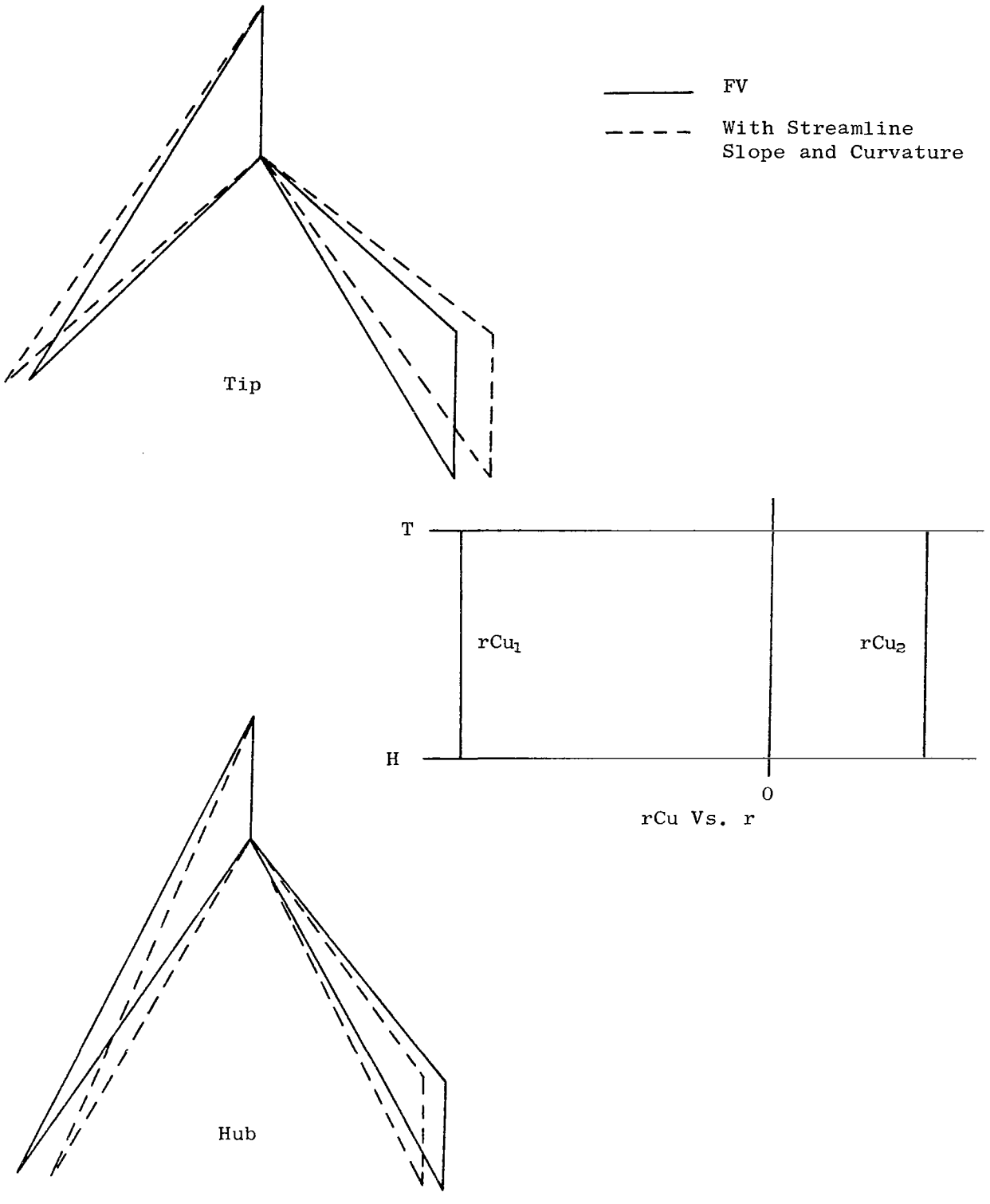

Figure 12. Constant-Outside-Diameter Flowpath Streamline Slope and Curvature Effect Compared to Free Vortex for Typical Stage One.

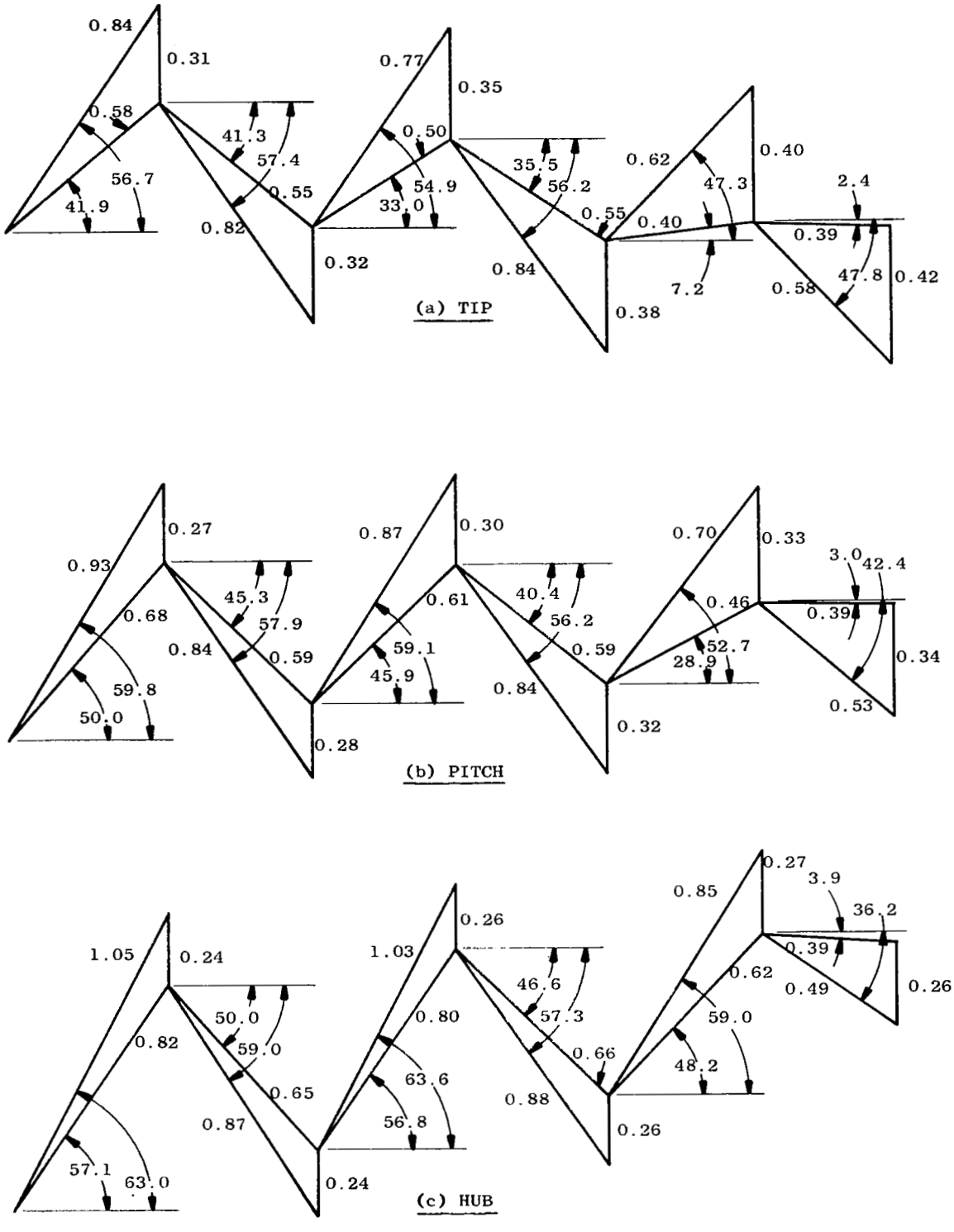

Figure 13. Scaled Vector Diagram for Stage One ψ_p = 20% Δh on Stage Three (Case 15).